DEGREE PROJECT IN MECHANICAL ENGINEERING,
SECOND CYCLE, 30 CREDITS
STOCKHOLM, SWEDEN 2020

Numerical optimization of solar sail trajectories to Mars

GUILLERMO JOSÉ MARTÍNEZ CABALGA

KTH ROYAL INSTITUTE OF TECHNOLOGY
SCHOOL OF ENGINEERING SCIENCES

Numerical optimization of solar sail trajectories to Mars

Guillermo José Martínez Cabalga

A thesis presented for the degree of
Master's of Science in Aerospace Engineering

Supervisor: Christer Fuglesang
Kungliga Tekniska Högskolan
School of Engineering Sciences
Stockholm
Sweden
10/09/2020

Abstract

Typical propulsion systems for space transportation involve the ejection of mass for momentum gain. Solar sails remove the requirement for propellant mass by obtaining their momentum from solar photons, which requires large surface area and very low mass. In this way solar sailcraft generate constant accelerations, in contrast with the impulsive thrust of chemical rockets. This enables new families of orbits and presents a new challenge for optimization and control. This study presents a summary of proven solar sail technology and investigates minimum-time trajectories to and from Mars. This optimization is carried out in two phases, using an energy rate-maximizing algorithm for planetary escape and sparse nonlinear programming for the interplanetary segment. The results provide upper bounds for minimum-time transfers and are then compared to possible sail sizes and sailcraft masses. This in turn may inform the design and selection of future missions for materials exchange during exploration or settlement efforts.

Sammanfattning

Typiska framdrivningssystem för rymdtransport involverar utkast av massa för momentumförstärkning. Solsegelr tar bort kravet på drivmassa genom att ta kraft från solfotoner, vilket kräver stor yta och mycket låg massa. På detta sätt genererar solsegelfarkoster konstant acceleratione, i motsats till kemiska raketers impulsiva dragkraft. Detta möjliggör nya familjer av banor och utgör en ny utmaning för optimering och kontroll. Denna studie presenterar en sammanfattning av beprövad solsegelteknologi och undersöker minimitidsbanor till och från Mars. Denna optimering utförs i två faser med hjälp av en algoritm som maximerar energiökningen för planetflykt gles gles olinjär programmering (eng: sparse nonlinear programming) för det interplanetära segmentet. Resultaten ger övre gränser för minimal tid för resorna och jämförs sedan med möjliga segelstorlekar och massor för segelfarkosterna. Detta kan i sin tur ge information om utformningen och valet av framtida rymdfärder för lasttransporter vid utforskning eller bosättning.

Contents

1 Introduction

From simple rafts and canoes, through triremes and galleons, to oil tankers and aircraft carriers, transportation technologies have continuously evolved to enable faster, more efficient travel. Every vehicle is designed for one or several purposes, adapting to its target environment. In the field of space travel we have almost exclusively developed propulsive means of travel, which receive their momentum directly from pushing matter away.

Thanks to the high levels of thrust that rocket engines can provide, this will likely remain the only feasible way of escaping deep gravitational fields for a long time. However, once a vehicle is in orbit, the requirement for high, short-lived thrust becomes less meaningful, and opportunities arise for alternative means of 'propulsion'. We desire to maximize the amount of mass that rockets can put in orbit, and in the case of interplanetary travel, much of this mass is just fuel. This thesis explores a concept that requires no fuel and instead utilizes the physical environment in interplanetary space: solar sails. Much like sailboats don't need to burn oil, solar sails require no rocket fuel.

1.1 Motivation

Effective interplanetary travel is essential for the exploration of the Solar System, and even more for humankind's eventual expansion into permanent or semi-permanent settlements on other planets. Approximately seven tons of fuel are required to bring one ton of payload from low Earth orbit (LEO) to an orbit around Mars. Even considering a highly autonomous settlement capable of manufacturing most of its required materials directly from in-situ resources, shipping routes will be necessary, but cutting down fuel costs will be key.

For example, the first Mars settlements will likely be able to use Martian regolith (dust and soil) for construction and manufacturing of tools, and even synthesize rocket fuel from local water deposits. However, they will not be able to craft specialized electronics or highly-advanced synthetic materials, which will then need to be imported from Earth.

Moreover, two of the main reasons to go to Mars—or any other planet or asteroid—are scientific research and resource mining. In the first case only small samples might be gathered, but the purpose of mining will be to return resources for their use on Earth. The time of travel for both cases will not necessarily be a constraint, but the goal will be to minimize cost, and therefore fuel. Solar sails, while slow, require no fuel for their operation, and are thus an attractive concept to establish such trade routes.

In addition to shipping routes, solar sails can be used for specialized missions that require constant thrust. More details are given in the following sections.

2 Solar Sails

2.1 Overview

A solar sail is, to all effects, just a large surface. It gains momentum by reflecting photons, usually from the light of the Sun. Most satellites, especially those on sun-synchronous orbits, experience this as a force acting on their exposed area, called solar radiation pressure (SRP). Since most artificial satellites are very

dense, the resulting force is small, but over time it becomes non-negligible and needs to be corrected. A solar sail instead aims to have as much exposed area as possible to the SRP while being as light as possible in order to achieve a high enough acceleration.

An essential difference between solar sails and rocket engines is the time of actuation of thrust. Chemical engines provide large amounts of thrust in a very short time. Solar sails, or sailcraft hereafter, typically have much smaller accelerations, extended over a long period of time—in fact, a solar sail can have a constant acceleration, although not necessarily uniform. Besides the evident differences in terms of fuel, such a long-drawn acceleration allows for distinct maneuvering and unlocks the possibility of entering non-Keplerian, non-periodic orbits. Non-Keplerian orbits are orbits that take place in three dimensions rather than on a plane. Solar sails enable displaced orbits: circular, Sun- or planet-centered orbits displaced from the ecliptic plane, which could have unique applications in solar physics, space weather, and planetary observation missions [1]. At any rate, these considerations are beyond the scope of this thesis.

2.2 History

Solar radiation pressure, while not entirely understood at the time, was already conjectured in 1619 by none other than Johannes Kepler. He proposed that sunlight pushes comet tails outward. However, it wasn't until 1873, when James Clark Maxwell proposed his famous set of equations [2], that SRP received a theoretical explanation from physical principles. A few years later science fiction authors began writing about mirror spaceships, a concept later picked up by Herman Julius Oberth to illuminate Earth's northern reaches, and eventually extended into applications of orbit transfer, maneuvering and control [3].

Despite this foundation along with the work of Konstantin Tsiolkovsky and other rocket scientists [4–6], there were not any notable inquiries into the concept for several decades. Finally, in the 1970s, NASA's Jet Propulsion Laboratory (JPL) conducted a conceptual study of several possible designs for a rendezvous mission with Halley's Comet in 1986. The final design was a 0.6 km^2 sail. The project was cancelled in 1977, but the study provided a solid foundation for many later studies [7, 8]. Since then several solar sails have flown successfully (see table 1). One of the most advanced missions currently under development is OKEANOS, by the Japan Aerospace Exploration Agency (JAXA). Its goal is to retrieve samples from asteroids in the same orbit as Jupiter, scheduled to launch in 2026. In an interesting development, the 1,600 m^2 sail is also capable of generating energy, like a solar panel. At any rate, OKEANOS will also incorporate an ion engine to aid in its propulsion [9, 10].

In summary, although the concept of solar sails has been present for over a century, the last ten years have seen great strides made towards functional utilization of sails as means of long-distance travel. Before discussing the state of the art of sail crafting, a brief explanation of the mechanics of sails will be presented.

2.3 Mechanics of Solar Sails

Solar sails gain their energy via collisions from photons, which are reflected away from the surface. For simplicity, this study will focus on ideal sails, where

Table 1: Past and future solar sail missions.

Launch date	Agency	Mission Name	Goal	Design/test level	Sail size (m^2)	β	Notable features
1977	JPL	-	Rendezvous with Halley's Comet	Concept study	6.4×10^5	0.175	Spin-stabilized 4 ton heliogyro carrying a 800kg conventional spacecraft
1999	DLR-ESA-INVENT	ODISSEE spin-off	Feasibility demonstration	Ground Test	330	0.044	Deployment successful in simulated $0g$ using helium balloons; stored volume $0.19m^3$.
2004	NASA for ATK and L'Garde	-	Development and ground testing	Prototypes deployed, functional vacuum testing	400	0.003	Two successful independent prototypes, ATK's including 130kg bus and payload
2005	Planetary Society	Cosmos-1	Technology validation	Launch vehicle failure	600	0.009	Launched from a Russian submarine
2010	JAXA	IKAROS	Research	Mission success; end of mission in 2015	196	0.001	Solar cells and liquid crystals for AOCS
2011	NASA	NanoSail-D2	Technology validation	Launch successful, control lost	10	0.004	3U CubeSat; designed to burn up within 120 days but took 240 days
2015	Planetary Society	LightSail 1	Technology validation	Test flight successful	32	0.011	Follow-up to Cosmos-1; CubeSat 3U platform
2019	Planetary Society	LightSail 2	Technology validation	Currently in-flight	32	0.010	CubeSat 3U platform; orbit raised by a "measurable" amount
2021	NASA	Near Earth Asteroid Scout	Technology validation, asteroid study	Planned	86	0.009	CubeSat 6U; to be launched on Space Launch System (SLS)
2026	JAXA	OKEANOS	Asteroid study and sample return	Planned	1600	0.002	Hybrid sail/panel for propulsion and electric power plus ion engine; possible asteroid lander

the assumption is that photons are reflected specularly, resulting in a force perpendicular to the sail surface. In reality, imperfections on the surface and sail billowing will cause photons to scatter in a range of directions, reducing the resulting thrust [11]. This effect is typically very small, so it is suitable to ignore it for the purposes of this study.

As shown in figure 1, a sail surface with normal vector $\boldsymbol{n}$ and area A under a photon pressure P experiences a force due to the incident photons given by

$$\boldsymbol{f}_i = PA(\boldsymbol{u}_i \cdot \boldsymbol{n})\boldsymbol{u}_i \tag{1}$$

where $A(\boldsymbol{u}_i \cdot \boldsymbol{n})$ is the sail surface projected in the direction of $\boldsymbol{u}_i$. In addition, the reflected photons exert an equal force in the specular reflected direction $-\boldsymbol{u}_r$:

$$\boldsymbol{f}_r = -PA(\boldsymbol{u}_i \cdot \boldsymbol{n})\boldsymbol{u}_r \tag{2}$$

These can be combined using the vector identity $\boldsymbol{u}_i - \boldsymbol{u}_r = 2(\boldsymbol{u}_i \cdot \boldsymbol{n})\boldsymbol{n}$ to yield

$$\boldsymbol{f} = 2PA(\boldsymbol{u}_i \cdot \boldsymbol{n})^2\boldsymbol{n} \tag{3}$$

Then, for an incidence angle α, the acceleration on the sail becomes

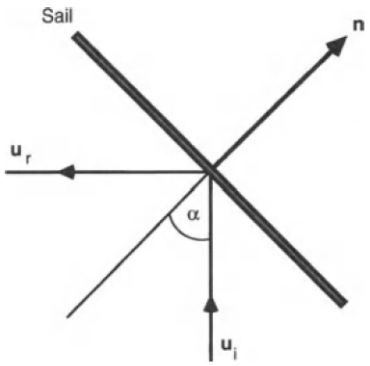

Figure 1: Incident and reflected photon streams on a solar sail [11].

$$\boldsymbol{a} = \frac{2\eta P}{\sigma} \cos^2 \alpha \, \boldsymbol{n}, \tag{4}$$

where η denotes the solar sail efficiency (unity in the case of an ideal sail) and $\sigma = m/A$ is the mass-to-area ratio, also called sail loading or sailcraft areal density. The solar radiation pressure varies with distance from the Sun following an inverse square law,

$$P = P_0 \left(\frac{R_0}{r} \right)^2 \tag{5}$$

so a typical parameter to describe sailcraft is the characteristic acceleration a_c, which is calculated using the pressure at the Earth's average distance from the Sun (1 astronomical unit):

$$a_c = \frac{2P_\oplus}{\sigma} \tag{6}$$

where the SRP at Earth's distance from the Sun is measured as $P_\oplus = 9.12 \cdot 10^{-6}$ N m^{-2}. The characteristic acceleration is usually expressed in millimeters per second squared. In order to avoid confusion, an equivalent but dimensionless parameter can be used. The lightness number β is defined as the ratio of solar radiation pressure acceleration to the solar gravitational acceleration:

$$\beta = \frac{2PR^2}{\sigma \mu_\odot}, \tag{7}$$

where $R_\oplus$ is the distance between the Sun and the Earth and $\mu_\odot$ is the gravitational parameter of the Sun. Both β and a_c contain the information required to calculate the dynamics of a sail in space regardless of the sail's configuration and mass distribution.

Combining equations 4 and 7, the acceleration vector due to SRP becomes

$$\boldsymbol{a_s} = \beta \frac{\mu_\odot}{r_s^2} (\hat{\boldsymbol{r}}_{\boldsymbol{s}} \cdot \hat{\boldsymbol{n}})^2 \, \hat{\boldsymbol{n}}, \tag{8}$$

where $\boldsymbol{r_s}$ is the vector from the Sun to the sail and $\hat{\boldsymbol{n}}$ is the unit vector normal to the sail's surface.

2.4 State of the Art

Attitude Control

One important aspect of sail mechanics evidenced by equation 8 is that the direction of the acceleration depends on the attitude of the sail. As will be shown later, interplanetary trajectories are usually smooth enough that a small torque can produce the desired orientation in an appropriate time. There exist two main concepts for attitude control. The more traditional method consists of tip-mounted vanes, small sections of sail that can be actuated into a desired orientation. This effectively changes the exposed area of the sail as well as shifting the center of mass, resulting in controllable torque. These mechanisms, while conceptually simple, increase the structural complexity of the sail, and can lead to problematic vibration modes. Moreover, the mechanism itself adds mass to the sail structure.

A more novel yet already demonstrated control system is that used in IKAROS: liquid crystal devices. These are small panels embedded in the sail whose reflectance can be adjusted electronically. As they use sunlight pressure to generate a constant torque, they avoid causing vibrations on the membrane [12, 13].

Both of these systems can be used to achieve three-axis stabilization, but most solar sails are also spin-stabilized for two main reasons. On one hand, it is a simple method that requires no extra propellant or mass from reaction wheels and therefore eases the requirements for the control systems. In addition, the centrifugal forces from the spinning help deploy and maintain the sail flat ant taut, such that its exposed surface is maximized.

Structure and materials

Besides attitude control systems, the structure of a sail consists of two main parts: a thin, lightweight membrane that provides the surface area, and booms to hold its structure and keep it from folding and billowing. Figure 2 shows the three main configurations that have been explored: square sails, with four diagonals masts and four triangular sail sections; heliogyro sails, consisting of several vanes rolled out from a central hub, and "ring" or spinning disk sails, which hold the sails taut against radiation pressure with masses along lines between sail sections [14].

Figure 2: Solar sail configurations.

Sail membranes are typically made of ultralight plastics such as Kapton or Mylar with areal densities between 3 and 20 g/m^2 [15]. A high-emissivity coating

is applied to the back side so as to maintain an appropriate thermal profile. Old designs of metallic booms had a density per unit length of about 50 g/m, but modern booms made of carbon fiber-reinforced plastics have drastically lowered this value to 15-25 g/m. In addition, their flexibility allows for them to be coiled about a central shaft, packed for launch.

It has been predicted that overall sail loading values, combining booms and membrane, could reach as low as 5 g/m^2 [16]. Using this number, figure 3 shows the change of β with increasing sail side length (assuming a square sail configuration) for various payload plus subsystems masses.

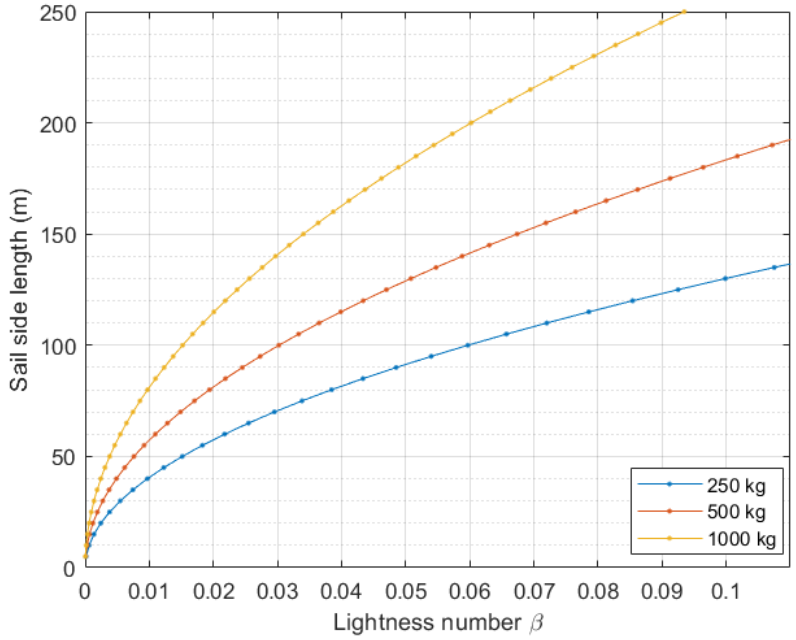

Figure 3: Evolution of lightness number with sail side length.

Packing, launch and deployment

A major challenge in sail design is to develop membranes and booms strong enough to withstand packing, launch and deployment. Evidently sails need to be packed into a compact state, since while extended they are larger than the cross-section of the fairing. The membranes must be folded and booms rolled, and then deployed via telescopic mechanisms. Coiled booms impose restrictions on their thickness and cross-section. Moreover, much of the sail film mass is taken up by substrates that provide sufficient tensile strength [17].

Sail size and scalability

There exist, in fact, physical limits for the payload mass fraction that result from the boom design constraints for packing and launch. In order to achieve

high β with heavy payloads, it is necessary to span as wide an area as possible. However, this in turn requires larger booms in all their dimensions: length, thickness and cross-section. The thickness, however, cannot be increased freely if the booms need to packed and later deployed. This results in a non-monotonic relationship between sail area and payload mass for fixed characteristic acceleration, as shown in figure 4.

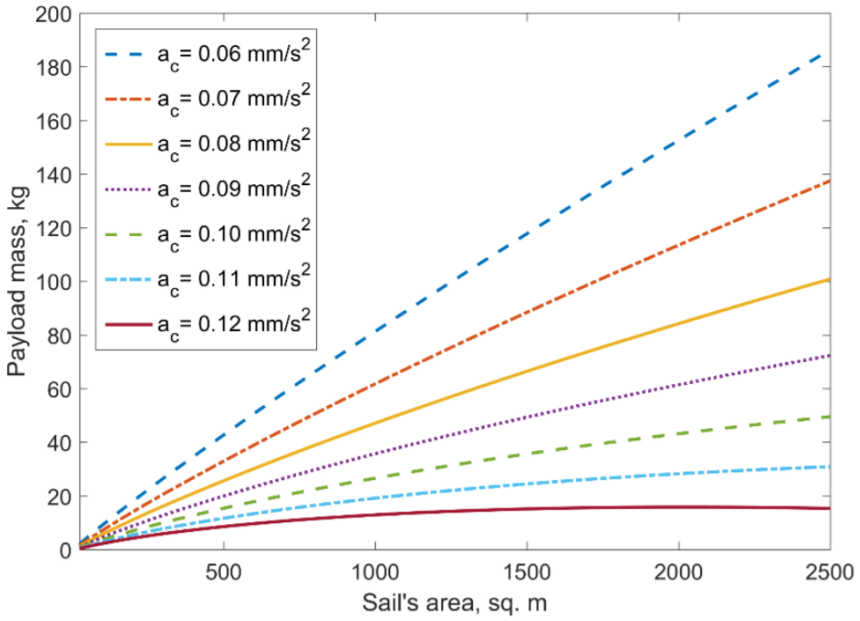

Figure 4: Relationship between payload mass and sail surface area [15].

This constraint may be circumvented with advanced designs for packing and deployment. However, combined with the challenges for membrane manufacturing, it is likely that the most effective method to construct robust sails for long-term missions will be on-orbit manufacturing.

2.5 On-Orbit Manufacturing and Assembly

Launcher constraints severely limit the kinds of structures and materials that can be brought to space. Engine ignition and shutdown, wind gusts, wind shear and other launch loads can induce very large stresses (vibratory or quasi-static) on payloads, which often need to be reinforced to withstand these forces. Also, as previously mentioned, there is only so much available space within rocket fairings, typically requiring the payload to be folded or otherwise compacted. Overall, there are several inherent problems with designing tools, vehicles and instruments that will be used exclusively in space, but need to be manufactured on Earth, such as scalability under gravity.

Despite great strides being made in terms of miniaturization and efficiency (for example, with solar panels), on-orbit manufacturing is the logical next step in the development of space infrastructure. The recent rise of cheap, reusable launchers opens up the possibility of bringing many components or modules

separately, and with technological advances in robotics and autonomous docking and rendezvous it is easier than ever to assemble large structures in space.

Studies have shown that on-orbit assembly, while incurring a high initial cost, will significantly reduce the costs and increase profits of space-based activities, be they Earth observation, solar and space physics, exploration, commercial missions and national security [18]. On-orbit manufacturing capabilities will enable restoring, re-purposing and upgrading existing space structures such as communications satellites or telescopes. The ability to assemble solar panels or antennae on-orbit means they need not be packed for launch, and therefore allows much larger systems to work together, providing greater power.

Moreover, zero-g manufacturing enables advanced materials that either cannot be made on Earth, or have inferior qualities. A suitable example is ZBLAN optical fiber. Its manufacturing process is hampered by crystallization resulting from gravity, and experiments aboard the International Space Station have successfully crafted fibers free of such defects [19, 20].

On-orbit manufacturing of solar sails would greatly reduce membrane mass required for packing and deployment [17], as well as avoid the payload mass fraction issues presented in [15].

3 Trajectory Optimization Method

3.1 Mission Goals

This thesis investigates optimal trajectories in the context of a cargo shipping route between Earth and Mars. Since solar sails require no fuel, the optimization variable here is time. The main target is therefore to minimize the time for one-way trajectories. This shall be done for a range of values for β, the dimensionless lightness number, in order to find trends and suitable ranges to aim for when designing a solar sail.

At any rate, optimal one-way trajectories need not be the optimal operations for a repeatable mission using the same spacecraft, since they require a specific constellation between the two planets (i.e. that their positions are in a particular phase with respect to each other). One of the advantages of solar sails, stemming from the lack of fuel, is the ability to select a trajectory after launch and design, whereas rockets need to ensure they have enough propellant. This freedom means that solar sails are not restricted by launch windows. Section 3.3.3 will provide proof-of-concept for this feature.

3.2 Assumptions

In order to simplify the problem, a number of assumptions have been made:

1. **The interplanetary orbits are two-dimensional.** Differences in orbital inclinations are disregarded with the understanding that they don't have a large effect on the time of flight of each mission. The planetary escape optimization method does use three dimensional orbits, however. In fact, it has been shown that three-dimensional trajectories are faster than two-dimensional ones [21], so the results of this study will be an upper bound of the attainable minima.

2. **Earth's and Mars' orbits are circular.** They are in fact elliptical, with eccentricities of 0.0167 and 0.0934 respectively, resulting in varying solar fluxes. These values are small, so their average semi-major axes will be used to define their radius.

3. **The size of the sphere of influence of the planets is negligible compared to their distance to the Sun.** The sphere of influence is used as an approximation of where a spacecraft exits a gravitational field and enters another. Naturally these fields coexist throughout space, but the approximation simplifies the unsolvable N-body problem to a 2-body problem, which can be solved analytically. The size of the sphere of influence of the Earth is only 0.6% of its distance to the Sun, so it is safe to disregard it for this study and assume that the interplanetary phase begins at a position equal to that of the planet.

4. **The only forces on the spacecraft are the solar radiation pressure and central body gravitation.** In reality there are other perturbing forces such as other bodies' gravitation,[1] oblateness effects, and interactions with the space environment, such as solar winds. These effects are, however, mostly negligible for the purposes and scope of this study.

5. **The solar sail will be capable to maneuver and reorient itself instantaneously.** The control histories resulting from the optimization are not continuous, but the optimal trajectories turn out to be smooth enough that demonstrated AOCS systems are sufficient.

6. **The sail behaves as an ideal sail.** As described in section 2.3, real sails experience accelerations tangent to the sail surface due to membrane imperfections. Moreover, real sails have a maximum cone angle (the angle between the photon stream and the sail force) of about 55 degrees, whereas for ideal sails this is extended to 90 degrees.

3.3 Optimization Problem

Each trajectory can be divided into two phases: the planetary escape, where the sailcraft is deep within the gravitational well of the Earth or Mars, and the interplanetary transfer, where the only gravitational force considered is that of the Sun. Upon arrival to the vicinity of the target, the strictly interplanetary segment ends, but in this study the capture is ensured directly as discussed below. In both phases the independent variable is the lightness number β, and the objective is to find minimum-time trajectories for each.

3.3.1 Planetary Escape: Maximum Orbital Energy Rate Transfer

The general equations of motion of a spacecraft in orbit around a central body are

$$\dot{\boldsymbol{r}} = \boldsymbol{v} \tag{9}$$

[1] Actually, the perturbing gravity of the Sun will be included when optimizing the planetary escape trajectories. However, the interplanetary transfer will ignore gravitational forces beyond that of the Sun.

$$\dot{\boldsymbol{v}} = \boldsymbol{g_c}(\boldsymbol{r}) + \boldsymbol{\Delta} \tag{10}$$

where $\boldsymbol{r}$ and $\boldsymbol{v}$ are the position and velocity vectors of the spacecraft relative to the central body (Earth or Mars in this case), $\boldsymbol{g_c}(\boldsymbol{r})$ is the gravitational acceleration and $\boldsymbol{\Delta}$ represents other the acceleration due to disturbing forces acting on the spacecraft. In this case, these will be the solar radiation pressure $\boldsymbol{S}$ and the gravitational perturbation of the Sun, $\boldsymbol{g_\odot}$:

$$\boldsymbol{\Delta} = \boldsymbol{S} + \boldsymbol{g_\odot} \tag{11}$$

The orbital energy and its time derivative are generally expressed as

$$E = \frac{1}{2}\boldsymbol{v}^T\boldsymbol{v} + U(\boldsymbol{r}) \tag{12}$$

$$\dot{E} = \dot{\boldsymbol{v}}^T\boldsymbol{v} + \frac{\partial U}{\partial \boldsymbol{r}}\dot{\boldsymbol{r}} \tag{13}$$

where $U(\boldsymbol{r})$ is the potential energy per unit mass in the gravitational field of the central body. Then, since $\boldsymbol{g}_c^T = -\partial U/\partial \boldsymbol{r}$ and plugging in equations 9 and 10:

$$\dot{E} = (\boldsymbol{g}_c + \boldsymbol{\Delta})^T\boldsymbol{v} - \boldsymbol{g}_c^T\boldsymbol{v} = \boldsymbol{\Delta}^T\boldsymbol{v} = \boldsymbol{S}^T\boldsymbol{v} + \boldsymbol{g}_\odot^T\boldsymbol{v} \tag{14}$$

Maximizing this rate gives a simple control law to increase the orbital energy, which corresponds to escaping the central body's gravitational well. This method does not yield actually optimal trajectories, since it is only a series of local optimizations that don't account for the entire trajectory. However, studies have shown that for sail characteristic accelerations in the range used for this study, this method yields near-minimum-time solutions [22]. The implementation of this method was done in Matlab and follows the algorithm described by Coverstone, Prussing and Garcia de Herreros [22, 23]. The outputs are the optimal trajectories, their duration, and the control histories.

In the calculation of optimal trajectories, the specific location of the sailcraft at the start is irrelevant, as only the distance to the central body matters. After finding the optimal escape trajectory, the starting phase or periapsis can be selected such that the trajectory ends with the spacecraft departing the planet in the desired direction (along the velocity of Earth when going to Mars, and against the velocity of Mars when returning to Earth). Therefore, the only relevant initial condition is the initial radius. For the Earth escape, this was set to 40,000 km in order to avoid the relatively densely populated geostationary orbits around 36,000 km. For the Mars escape segment, it was set to 6,779 km, double the planet's radius.

The final condition for this segment is that $E = 0$, corresponding to having fully escaped the planet's gravitation. In practice, this often results in excess energy, and therefore excess velocity v_∞ with respect to the planet. This value is then used as an initial condition for the interplanetary transfer.

3.3.2 Interplanetary transfer: PSOPT

Upon exiting the planet's gravitational well, the second part of the optimization begins. The only forces acting on the sailcraft in this segment are the solar radiation pressure and the gravitational pull from the Sun. The optimization is carried out using PSOPT, an open source optimal control software package

written in C++ that uses direct collocation methods, including pseudospectral and local discretizations [24]. The problem consists of a cost function, state and control vectors and equations, path constraints and event/boundary conditions.

The cost function is simply $J = t_f$, the final time when the final conditions are met. As the problem is implemented in only two dimensions, the state vector is

$$\boldsymbol{x} = [\boldsymbol{r} \quad \boldsymbol{v}] = [x \quad y \quad \dot{x} \quad \dot{y}]^T \tag{15}$$

where x and y are Cartesian coordinates in a heliocentric frame. The control vector can then be expressed as

$$\boldsymbol{u} = \boldsymbol{n} = [u_x \quad u_y]^T \tag{16}$$

This is the vector normal to the sail surface as introduced in section 2.3. Moreover, it is unitary, such that $\boldsymbol{n} = \hat{n}$.

The state equations define the system dynamics:

$$\dot{\boldsymbol{r}} = \boldsymbol{v} \tag{17}$$

$$\dot{\boldsymbol{v}} = [\ddot{x} \quad \ddot{y}]^T = \frac{\mu_\odot}{r^2} \cdot \beta \left(\hat{\boldsymbol{r}} \cdot \hat{\boldsymbol{u}}\right)^2 \hat{\boldsymbol{u}} - \frac{\mu_\odot}{r^2} \hat{\boldsymbol{r}} \tag{18}$$

where the first term is the solar radiation pressure as seen in equation 8, and the second term is the gravitational acceleration.

For the Earth-Mars transfer, the initial state vector is

$$\boldsymbol{x}_i = [R_\oplus \quad 0 \quad 0 \quad -(v_\oplus + v_\infty)] \tag{19}$$

where $R_\oplus$ and $v_\oplus$ are the distance and velocity of the Earth with respect to the Sun, respectively, and v_∞ is the excess velocity after escaping the planet, which is a result from the previous section. For the return trip, the initial conditions are then

$$\boldsymbol{x}_i = [R_\sigma \quad 0 \quad 0 \quad -(v_\sigma - v_\infty)] \tag{20}$$

where R_σ and v_σ are the distance and velocity of Mars, again with respect to the Sun. Since the goal is to slow down to return to Earth, v_∞ is opposite to the planet's translation. In both cases the planets are modeled to be moving in clockwise orbits.

Since this optimization is for the general case, it is not necessary to model the actual motion of the planets. Therefore the first final condition is set to $|\boldsymbol{r}_f| = R_\sigma$ or $|\boldsymbol{r}_f| = R_\oplus$. This condition alone, however, does not ensure capture, since the sailcraft may be too fast or too slow with respect to the target planet. Consequently the closest approach and corresponding velocity are found in order to calculate the sailcraft's energy with respect to the planet, such that the second final condition is that

$$E = \frac{v^2}{2} - \frac{\mu}{r} < 0 \tag{21}$$

for r and v relative to the target planet. Occasionally this results in large negative values, which would physically translate to very low final orbits. However, the actual value of the arrival energy is hugely dependent on the periapsis or

impact parameter, which is very sensitive to small changes throughout the trajectory. Therefore this matter is left as a standing issue that would realistically be addressed by course corrections.

Path constraints need to be set to ensure that the sailcraft orientation never exceeds 90°, as this would imply acceleration towards the Sun, and to maintain the control vector unitary. This can be done effectively by setting

$$\begin{aligned} \hat{r} \cdot \hat{\boldsymbol{u}} &\geqslant 0 \\ \boldsymbol{u} \cdot \boldsymbol{u} &= 1 \end{aligned} \tag{22}$$

Lastly, to ensure better convergence the optimization requires an initial guess. This was done by setting a linearly increasing radius and decreasing velocity between the desired endpoints (and vice-versa for the return trip), then extending this over the desired spiral segment. In this manner many optimizations can be run for a given β, running over a range of initial guesses parameterized by $C \cdot \pi$, with $0 < C \leqslant 10$. Geometrically this translates into spirals of varying length between two endpoints.

3.3.3 Target-time Transfer: Launch Window Removal

Launch windows are a major constraint for chemical rockets. In order to minimize fuel costs it is essential to follow close to optimal trajectories, which rely on the correct alignment between the starting and ending points. This limits the possible frequency of transfers: for example, a 9-month Hohmann transfer from Earth to Mars can only launch every 26 months. In contrast, a solar sail can use any possible trajectory without incurring extra fuel costs. In fact, if sailcraft operations are to be continuous (i.e. multiple back-and-forth trips), optimal operations will likely not rely on optimal single trajectories. After the first trip, Mars and Earth won't be in the right constellation for an optimal return trip. Instead of waiting for the right alignment, the sail can start on a sub-optimal return trajectory that will overall save time.

Due to computational and time constraints, this study will provide only a simple proof of concept. By altering only the cost function in the PSOPT implementation, it is possible to select trajectories with a desired time of flight. Let this time be t_{target}, then let the cost function be

$$J = (t_f - t_{\text{target}})^2 \tag{23}$$

where the square ensures that the target time can be approached both from above and below.

3.4 Analysis and post-processing

To ensure that the resulting trajectories and control histories are physically viable, a Matlab script was used to forward-propagate them independently of PSOPT. In addition, for each β, this script compares the optimizations resulting from different initial guesses, and identifies the corresponding minimum-time trajectory that correctly matches initial and final conditions.

4 Results

4.1 Planetary Escape

Table 2: Earth and Mars escape times (in days) for various lightness numbers.

β	0.005	0.010	0.015	0.020	0.025	0.030	0.035	0.040	0.045	0.050
$t_\oplus$	1908	973	678	565	409	344	314	262	234	268
t_σ	979	790	550	457	384	309	285	242	217	197
β	0.055	0.060	0.065	0.070	0.075	0.080	0.085	0.090	0.095	0.100
$t_\oplus$	194	177	192	161	142	134	127	118	122	106
t_σ	184	171	157	148	147	130	124	120	113	139

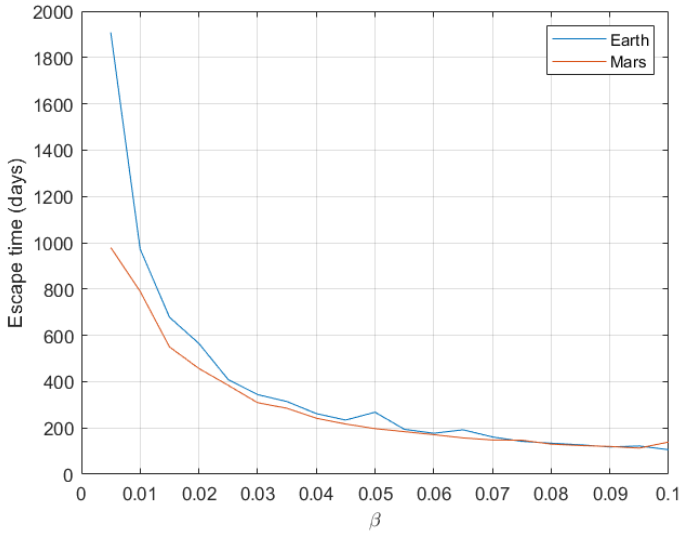

Figure 5: Escape times vs β for Earth (blue) and Mars (red).

Table 2 presents the times required to escape the Earth and Mars for $0.005 \leqslant \beta \leqslant 0.1$ using the method of maximizing the energy rate. Figure 5 shows that the time of flight decreases as a power law as the lightness number increases: fitting the data results in $t = 12.613 \times \beta^{-0.951}$ for Earth and $t = 19.282 \times \beta^{-0.785}$ for Mars. The small bumps at $\beta = 0.05$ and 0.065 are likely numerical anomalies in the optimization: as it depends on a number of variables such as integration time, there can be some variance between solutions.

Figures 6 and 7 each show two sample trajectories for $\beta = 0.1$ and $\beta = 0.01$. As expected, a larger β results in shorter time and fewer revolutions around the planet, as the sailcraft experiences a greater acceleration. Each of the trajectories shown here results in a final velocity vector in a different direction: this defines at what point in the starting orbit the sailcraft should depart, which should be chosen such that the final velocity is prograde when departing Earth and retrograde when escaping Mars.

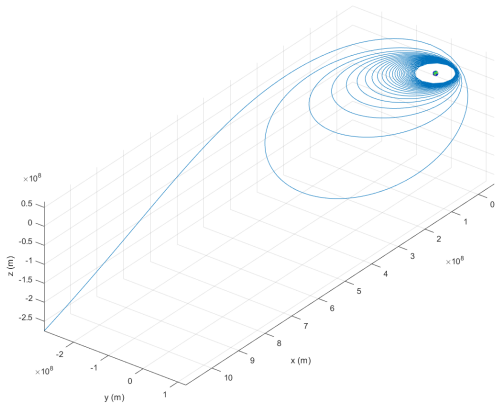

(a) $\beta = 0.1$, $t_{\text{escape}} = 106$ days

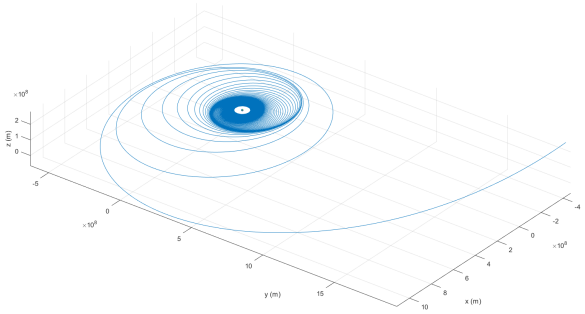

(b) $\beta = 0.01$, $t_{\text{escape}} = 1908$ days

Figure 6: Earth escape trajectories.

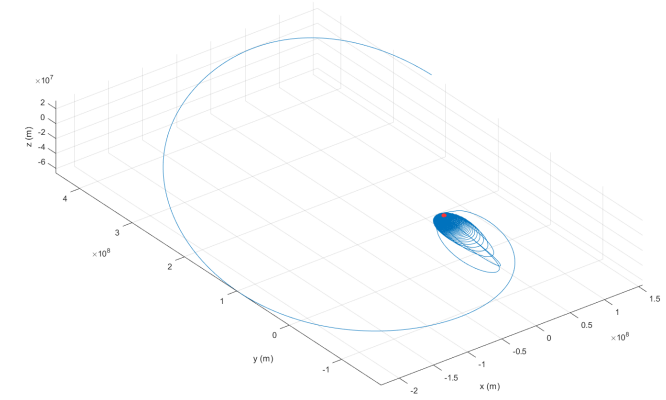

(a) $\beta = 0.1$, $t_{\text{escape}} = 139$ days

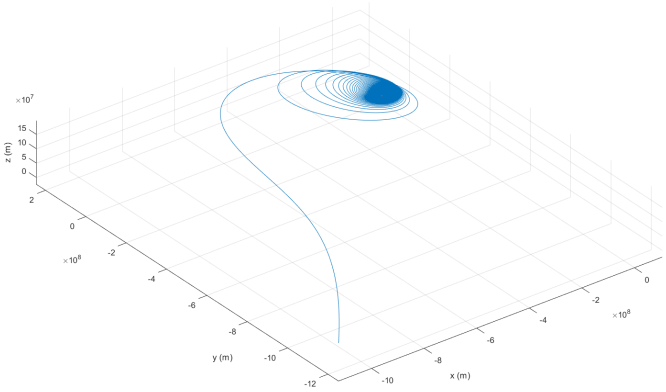

(b) $\beta = 0.01$, $t_{\text{escape}} = 979$ days

Figure 7: Mars escape trajectories.

4.2 Interplanetary Transfer

4.2.1 Earth to Mars transfer

The resulting transfer times for the Earth-Mars trip are shown in table 3, and three representative orbits are depicted in figures 8 to 10. Each of these transfers starts with a different velocity depending on the corresponding escape trajectory, which impacts their initial heliocentric orbit and therefore their duration.

Table 3: Earth to Mars transfer times (in days) for various lightness numbers.

β	0.005	0.010	0.015	0.020	0.025	0.030	0.035	0.040	0.045	0.050
$t_{\oplus-\sigma}$	-	-	1647	1157	778	727	591	283	293	267
β	0.055	0.060	0.065	0.070	0.075	0.080	0.085	0.090	0.095	0.100
$t_{\oplus-\sigma}$	265	253	213	209	212	197	190	188	192	176

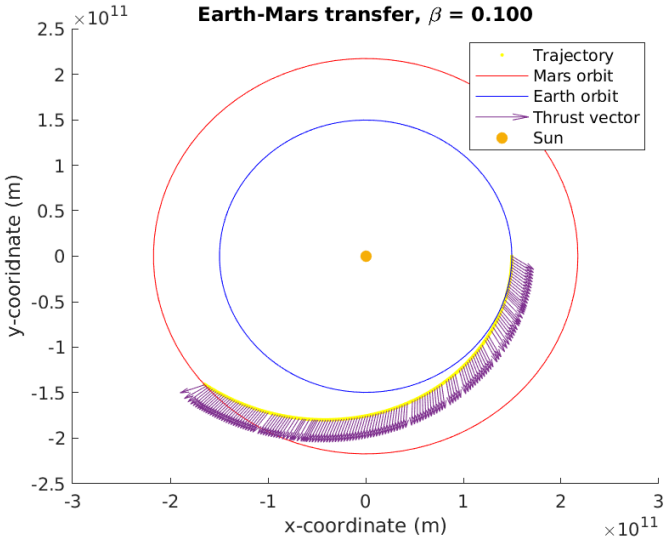

Figure 8: Earth-to-Mars transfer with $\beta = 0.1$ and $t_{\text{transfer}} = 176$ days.

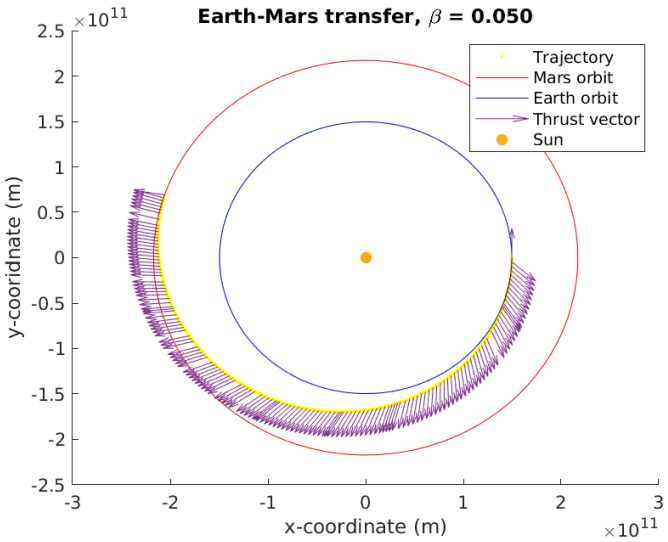

Figure 9: Earth-to-Mars transfer with $\beta = 0.05$ and $t_{\text{transfer}} = 267$ days.

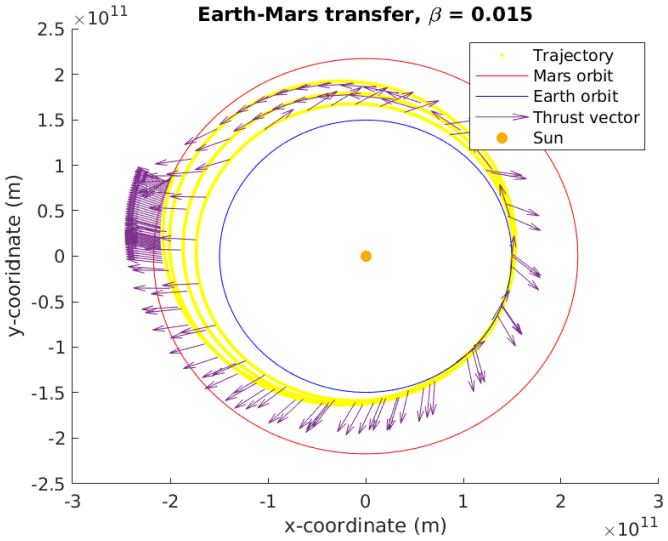

Figure 10: Earth-to-Mars transfer with $\beta = 0.015$ and $t_{\text{transfer}} = 1647$ days.

At high β the program converges quickly and easily, resulting in properly smooth trajectories. In contrast, figure 10 is less elegant. PSOPT automatically refines its mesh and increases the number of nodes or segments, resulting in many nodes in close proximity to Mars. Interestingly, after the first full orbit around the Sun, the sailcraft starts to brake after reaching apohelion, likely in order to maintain low perihelion and thus higher SRP.

4.2.2 Mars-to-Earth transfer

The return trip times are shown in table 4. Again, three representative orbits are presented in figures 11 to 13, which show the sail braking throughout most of the orbits.

Table 4: Mars to Earth transfer times (in days) for various lightness numbers.

β	0.005	0.010	0.015	0.020	0.025	0.030	0.035	0.040	0.045	0.050
$t_{\sigma-\oplus}$	-	-	778	774	1179	794	785	811	299	293
β	0.055	0.060	0.065	0.070	0.075	0.080	0.085	0.090	0.095	0.100
$t_{\sigma-\oplus}$	293	285	286	294	286	287	293	330	283	262

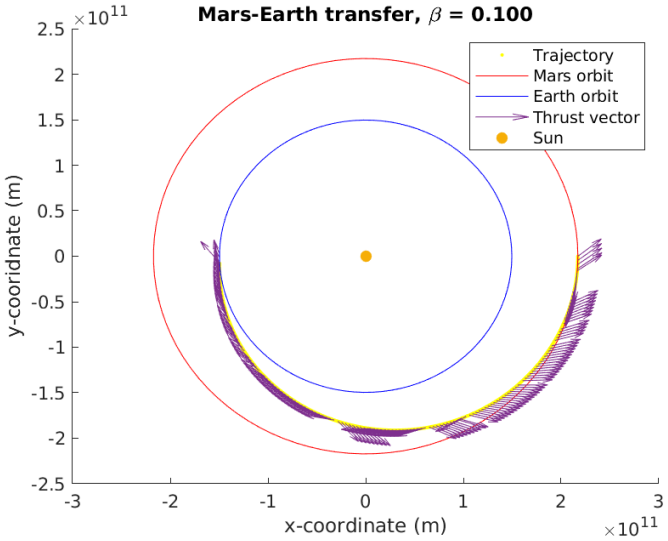

Figure 11: Earth-to-Mars transfer with $\beta = 0.1$ and $t_{\text{transfer}} = 262$ days.

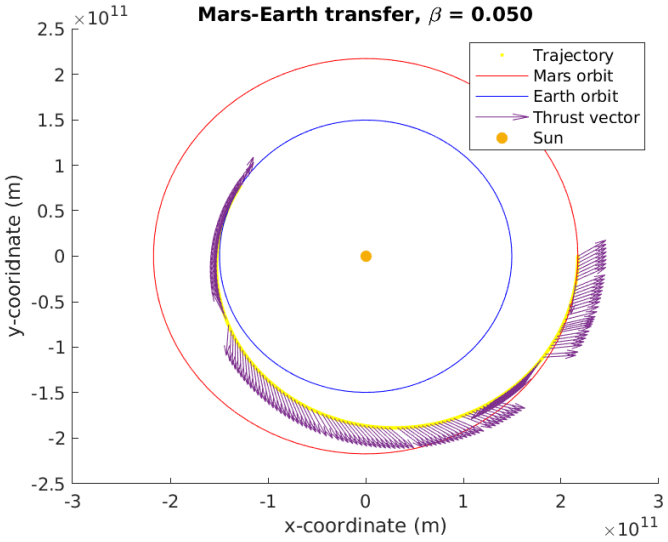

Figure 12: Earth-to-Mars transfer with $\beta = 0.05$ and $t_{\text{transfer}} = 293$ days.

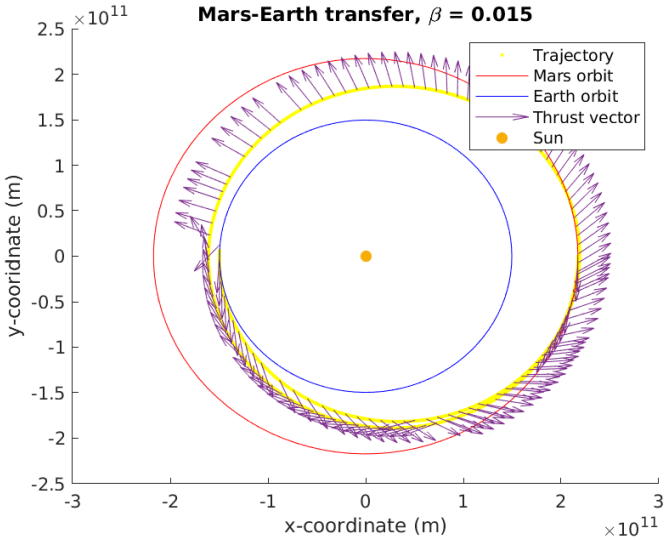

Figure 13: Earth-to-Mars transfer with $\beta = 0.015$ and $t_{\text{transfer}} = 778$ days.

4.3 Targeted Time of Flight

Figures 14 to 16 show three sample trajectories produced with PSOPT, optimized to reach a target mission duration with two different values of β. In particular, figure 14 shows a pattern of alternating prograde and retrograde acceleration, as would be intuitively expected.

These trajectories prove that it is possible for a solar sail to follow a sub-optimal trajectory to reach a desired target orbit, and that PSOPT has the capability to compute such trajectories.

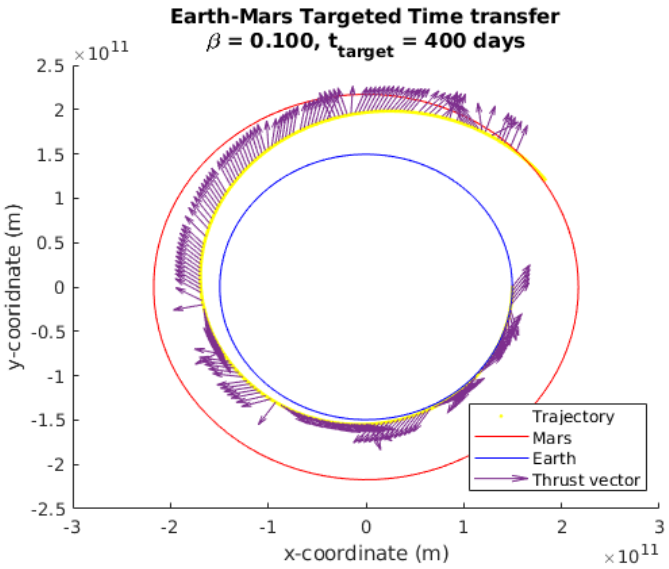

Figure 14: Earth-to-Mars fixed-time transfer with $\beta = 0.1$, $t_{\text{target}} = 400$ days and $t_{\text{transfer}} = 405$ days.

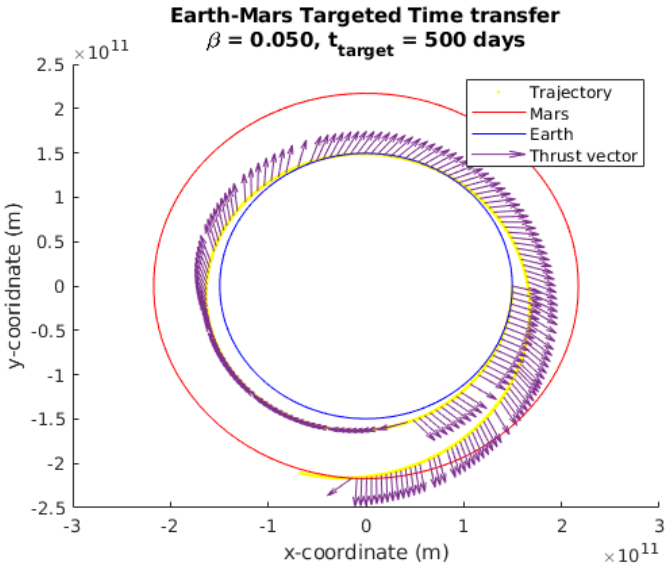

Figure 15: Earth-to-Mars fixed-time transfer with $\beta = 0.05$, $t_{\text{target}} = 500$ days and $t_{\text{transfer}} = 543$ days.

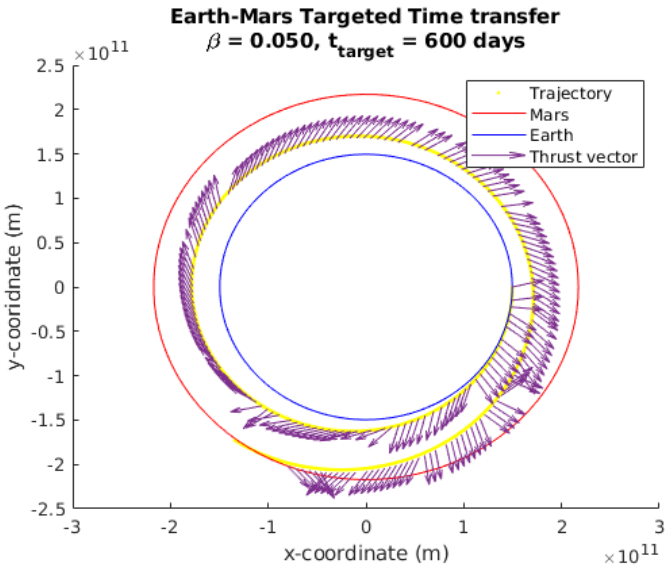

Figure 16: Earth-to-Mars fixed-time transfer with $\beta = 0.05$, $t_{\text{target}} = 600$ days and $t_{\text{transfer}} = 619$ days.

Naturally, these targeted-time trajectories need to be longer than the optimal time trajectories. It must be noted that the targeted times refer only to the interplanetary segment, with the escape segment left to calculate and design around. In any case, this serves as proof of concept, and further work can be done to refine and improve these results.

5 Discussion

As expected, the results above show that a lower lightness number results in longer transfer duration. Figure 17 shows the total times for each β and direction, including escape time and interplanetary transfer.

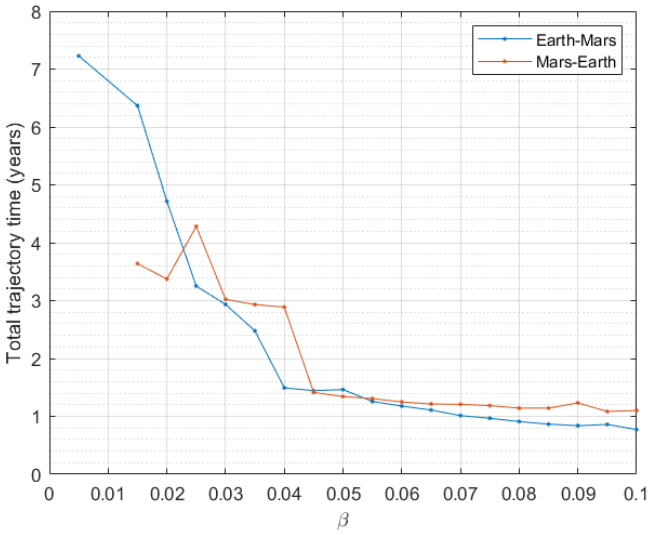

Figure 17: Total transfer times (escape plus interplanetary segment) for various β.

Despite a somewhat erratic behavior for low β (resulting from the difficulty to converge), the plot suggests an exponential relation between lightness number and total transfer time.

PSOPT is a powerful tool, but it can sometimes be fickle. In order to obtain good results with small β, a large number of computations need to be made, often with varying parameters (initial guess, number of nodes, etc). Due to time and technical constraints, some results are missing from tables 3 and 4.

To provide more context, figure 18 compares the required time of flight for one-way trips and side length for a square sail with various payload plus bus sizes. This was calculated from the data in figure 17 assuming a square sail with a membrane density of 2 g/m^2 and boom density of 15 g/m. It is immediately apparent that very large sails are essential for short missions with high payload capabilities.

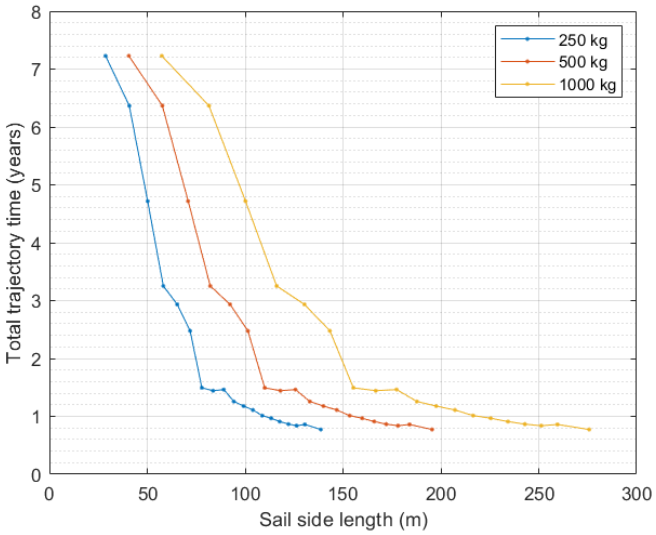

Figure 18: Total transfer Earth-Mars transfer times against side length for different payload-plus-bus masses.

Addressing assumptions

1. **3-D trajectories.** This thesis is limited to 2-dimensional trajectories for simplicity and technical constraints, but 3-dimensional transfers should in fact be faster. It has been previously demonstrated that applying the Pontryagin maximum principle results in shorter transfer times for non-planar trajectories [21].

2. **Elliptical orbits.** In reality, the distance between the Sun and the planets varies throughout the year, and so does the magnitude of the SRP. While the effects might be negligible for short, high-β transfers, the integrated effect over time would play a significant role, particularly during the escape segment [22].

3. **Orbital perturbations.** This study focuses solely on direct transfers, which are both flexible and simple to implement. However, for low β, other celestial bodies could be used to shorten the travel time via gravitational assists.

4. **Attitude control.** The results show mostly smooth orbits with few anomalies, with control segments far enough apart in time to allow existing attitude control systems to maneuver adequately.

5. **Ideal sail.** Most of the resulting control histories involve a large angle between the sail normal and the SRP, which would not result in the desired thrust with a real sail. This would mean that real transfers might be longer than found here, as the acceleration cannot be maximized in the desired direction.

6. **Initial conditions.** Where results were not found or were not satisfactory, it should still be possible to design appropriate missions if the initial conditions are changed. The simplest example would be to inject the sail in a transfer trajectory with chemical propulsion, therefore gaining velocity and reducing the total thrust that the sail would need to produce.

6 Conclusions

Evidently, sails with greater lightness numbers experience larger forces thanks to the SRP, and complete missions more quickly—in order to bring large payloads back and forth, a very large sail is essential. However, as the relation between time of flight and size appears to be exponential, it might not be necessary to strive for too large a sail, as it would result in only marginal gains. While more work needs to be done to refine the results above, judging from figure 17 an appropriate target could be the vicinity of $\beta = 0.06$. In this regime a one-way trip could take as little as 8 months, which is approximately equal to a Hohmann transfer. Although faster transfers can be achieved with other forms of propulsion, the cost savings over several trips can be enormous. In particular, the ability to maintain regular shipping routes and materials exchanges would be invaluable for settling, exploration and exploitation efforts.

Moreover, whereas traditional chemical and electrical engines need to carry excess fuel for maneuvers, solar sails can alter their course at any time without requiring extra mass, which allows them to expand or even do away with launch windows.

This thesis has only explored travel to Mars, but the same method could be adapted for travel to the Moon to aid in the Artemis program, or to asteroids for resource mining. There are plenty of opportunities for solar sailing to become a significant propulsion method, and they are currently mostly limited by available funding.

7 Future work

The first line of work to continue this study would be to improve and refine the optimization, changing parameters and using different built-in numerical methods. If the technical challenges can be solved, it should be possible to extend the PSOPT implementation to 3 dimensions, and even to include other celestial bodies and oblateness effects as perturbative force fields. A yet more rigorous implementation might even be able to work out gravitational assists on the Moon, Earth or the inner planets, which would be of particular interest if using smaller sails. Targeted-time trajectories can be explored in more depth, starting from the planetary escape segment, and refined to find more accurate results.

Still, the most important challenge facing solar sails is their construction. From perfecting materials and production to enabling assembly of large structures, much remains to be done before a solar sail can deliver significant payloads to Mars and beyond.

References

[1] Colin R McInnes. "Solar sail mission applications for non-Keplerian orbits". en. In: *Acta Astronautica*. Third IAA International Conference on Low-Cost Planetary Missions 45.4 (Aug. 1999), pp. 567–575. ISSN: 0094-5765. DOI: 10.1016/S0094-5765(99)00177-0. URL: http://www.sciencedirect.com/science/article/pii/S0094576599001770 (visited on 07/28/2020).

[2] James Clerk Maxwell. *A Treatise on Electricity and Magnetism*. en. Google-Books-ID: gokfAQAAMAAJ. Clarendon Press, 1873.

[3] Hermann Oberth. *Die Rakete zu den Planetenrãumen*. R. Oldenbourg, 1923.

[4] Konstantin Eduardovich Tsiolkovsky. "Exploration of the universe with reaction machines". In: *The Science Review* 5 (1903).

[5] Friedrich Tsander. "From a scientific heritage". In: *NASA Technical Translation No. TTF-541, NASA* (1967).

[6] Konstantin Eduardovich Tsiolkovsky. "Extension of man into outer space". In: *Proceedings of Symposion Jet Propulsion No. 2* (1936).

[7] *The Story of LightSail, Part 1*. en. URL: https://www.planetary.org/sci-tech/the-story-of-lightsail-part-1 (visited on 08/31/2020).

[8] Shengping Gong and Malcolm Macdonald. "Review on solar sail technology". en. In: *Astrodynamics* 3.2 (June 2019), pp. 93–125. ISSN: 2522-008X, 2522-0098. DOI: 10.1007/s42064-019-0038-x. URL: http://link.springer.com/10.1007/s42064-019-0038-x (visited on 07/28/2020).

[9] Osamu Mori et al. "Direct Exploration of Jupiter Trojan Asteroid using Solar Power Sail 1". In: 2016.

[10] Takahiro Iwata et al. "Investigation of the Solar System Structure using the Solar Power Sail: OKEANOS". In: 42 (July 2018). Conference Name: 42nd COSPAR Scientific Assembly, B1.1–65–18. URL: http://adsabs.harvard.edu/abs/2018cosp...42E1576I (visited on 07/30/2020).

[11] Colin R. McInnes. *Solar Sailing: Technology, Dynamics and Mission Applications*. en. Google-Books-ID: vfMilANfARYC. Springer Science & Business Media, Feb. 2004. ISBN: 978-3-540-21062-7.

[12] Yuichi Tsuda et al. "Achievement of IKAROS — Japanese deep space solar sail demonstration mission". en. In: *Acta Astronautica*. 7th IAA Symposium on Realistic Advanced Scientific Space MissionsAosta, Italy, July 2011 82.2 (Feb. 2013), pp. 183–188. ISSN: 0094-5765. DOI: 10.1016/j.actaastro.2012.03.032. URL: http://www.sciencedirect.com/science/article/pii/S0094576512001348 (visited on 08/31/2020).

[13] *IKAROS Small Scale Solar Powered Sail Demonstration Satellite | Spacecraft*. en. Library Catalog: www.isas.jaxa.jp. URL: http://www.isas.jaxa.jp/en/missions/spacecraft/current/ikaros.html (visited on 07/29/2020).

[14] *Solar Sail Technology Development*. Mar. 2005. URL: https://web.archive.org/web/20050311004606/http://solarsails.jpl.nasa.gov/introduction/design-construction.html (visited on 08/04/2020).

[15] Sergey P. Trofimov and Mikhail Yu. Ovchinnikov. "Performance Scalability of Square Solar Sails". In: *Journal of Spacecraft and Rockets* 55.1 (2018). Publisher: American Institute of Aeronautics and Astronautics _eprint: https://doi.org/10.2514/1.A33894, pp. 242–246. ISSN: 0022-4650. DOI: 10.2514/1.A33894. URL: https://doi.org/10.2514/1.A33894 (visited on 08/04/2020).

[16] Salama Moktar, Colin McInnes, and Patricia Mulligan. "Gossamer Sailcraft Technology". In: *Gossamer Spacecraft: Membrane And Inflatable Structures Technology For Space Applications*. American Institute of Aeronautics and Astronautics, pp. 481–501. ISBN: 978-1-56347-403-3. DOI: 10.2514/5.9781600866616.0481.0501. URL: https://arc.aiaa.org/doi/abs/10.2514/5.9781600866616.0481.0501 (visited on 08/04/2020).

[17] J. M. T. Thompson and Colin R. McInnes. "Solar sailing: mission applications and engineering challenges". In: *Philosophical Transactions of the Royal Society of London. Series A: Mathematical, Physical and Engineering Sciences* 361.1813 (Dec. 2003), pp. 2989–3008. DOI: 10.1098/rsta.2003.1280. URL: https://royalsocietypublishing.org/doi/10.1098/rsta.2003.1280 (visited on 07/28/2020).

[18] Iain D. Boyd et al. *On-Orbit Manufacturing and Assembly of Spacecraft*. Tech. rep. Institute for Defense Analyses, 2017, pp. i–ii. DOI: 10.2307/resrep22854.1. URL: https://www.jstor.org/stable/resrep22854.1 (visited on 08/31/2020).

[19] *Exotic Glass Fibers From Space:* en-US. Library Catalog: upward.issnationallab.org. URL: https://upward.issnationallab.org/the-race-to-manufacture-zblan/ (visited on 08/05/2020).

[20] Michael Johnson. *Made in Space—Building a Better Optical Fiber*. und. Text. Library Catalog: www.nasa.gov. Mar. 2019. URL: http://www.nasa.gov/mission_pages/station/research/news/b4h-3rd/eds-mis-building-better-optical-fiber (visited on 08/05/2020).

[21] Michiel Otten and Colin R. McInnes. "Near Minimum-Time Trajectories for Solar Sails". In: *Journal of Guidance, Control, and Dynamics* 24.3 (2001). Publisher: American Institute of Aeronautics and Astronautics _eprint: https://doi.org/10.2514/2.4758, pp. 632–634. DOI: 10.2514/2.4758. URL: https://doi.org/10.2514/2.4758 (visited on 08/25/2020).

[22] Victoria L. Coverstone and John E. Prussing. "Technique for Escape from Geosynchronous Transfer Orbit Using a Solar Sail". In: *Journal of Guidance, Control, and Dynamics* 26.4 (July 2003), pp. 628–634. DOI: 10.2514/2.5091. URL: https://arc.aiaa.org/doi/10.2514/2.5091 (visited on 07/28/2020).

[23] Maria Garcia de Herreros Miciano. "Feasibility study of the implementation of a space sunshade near the first Lagrangian point". MA thesis. KTH, Space Technology, 2020, p. 67.

[24] Victor M. Becerra. "Solving complex optimal control problems at no cost with PSOPT". In: *2010 IEEE International Symposium on Computer-Aided Control System Design*. ISSN: 2165-302X. Sept. 2010, pp. 1391–1396. DOI: 10.1109/CACSD.2010.5612676.

TRITA TRITA-SCI-GRU 2020:310